Lenisa *et al. EPJ Techniques and Instrumentation* (2019) 6:2
https://doi.org/10.1140/epjti/s40485-019-0051-y

EPJ Techniques and Instrumentation
a SpringerOpen Journal

EPJ.org

RESEARCH ARTICLE Open Access

Low-energy spin-physics experiments with polarized beams and targets at the COSY storage ring

P. Lenisa[1*], F. Rathmann[2], L. Barion[1], S. Barsov[3], S. Bertelli[1], V. Carassiti[1], G. Ciullo[1], M. Contalbrigo[1], A. Cotta Ramusino[1], S. Dymov[1,4], R. Engels[2], D. Eversheim[5], R. Gebel[2], K. Grigoryev[2], J. Haidenbauer[2,6], V. Hejny[2], H. Jagdfeld[7], A. Kacharava[2], I. Keshelashvili[2], A. Kononov[1], T. Krings[2], A. Kulikov[4], A. Lehrach[2], B. Lorentz[2], N. Lomidze[8], G. Macharashvili[8], R. Malaguti[1], S. Martin[9], S. Merzliakov[2,4], S. Mikirtychiants[3], A. Nass[2], N.N. Nikolaev[10], A. Pesce[1], D. Prasuhn[2], L. Semke[7], S. Squerzanti[1], H. Soltner[7], M. Statera[1], E. Steffens[11], H. Ströher[2], M. Tabidze[8], G. Tagliente[12], P. Thörngren-Engblom[13], S. Trusov[14], Yu. Uzikov[4,15,16], Yu. Valdau[2], C. Weidemann[2], P. Wüstner[17] and P. Zupranski[18]

*Correspondence: lenisa@fe.infn.it
[1]Universitá di Ferrara and INFN, 44122 Ferrara, Italy
Full list of author information is available at the end of the article

Abstract

A low-energy spin-physics program is being developed at the COSY storage ring. To support the planned experimental activities, several experimental tools for polarized beams and targets have been developed. The paper presents the physics case and the readiness of the setup for its realization.

Keywords: Polarized beams, Particle accelerators, Storage rings, Beam handling, Solid-state detectors

PACS: 29.27.Hj Polarized beams, 29.20.D Cyclic accelerators and storage rings, 29-27-Eg Beam handling, 25.43.+t Antiproton-induced reactions, 29.40.Wk Solid-state detectors

Introduction

Although the hadron physics program has been officially terminated [1], various experimental activities are underway at the COSY storage ring of Forschungszentrum Jülich. Besides the feasibility studies related to the search for electric dipole moments [2], low-energy spin-physics experiments employing polarized beam and targets appear as an additional focus. This paper is devoted to these studies.

One objective of the investigations is the completion of the studies devoted to the identification of a viable method to produce an intense beam of polarized antiprotons undertaken some years ago by the PAX Collaboration [3]. After having successfully performed a spin-filtering test with protons using a transversely polarized hydrogen gas target [4], the PAX Collaboration plans to complete these studies with a test of the longitudinal polarization buildup at COSY. The outcome of these studies will be of utmost importance for the possible application of polarized antiprotons at the FAIR[1] facility in Darmstadt.

[1]Facility for Antiproton and Ion Research https://fair-center.eu

A second physics goal consists of a time-reversal invariance test accessing the null-test observable $A_{y,xz}$ by scattering a vector polarized stored proton beam off a tensor polarized deuterium gas target [5]. The experiment proposed at the COSY storage ring promises to improve the present upper limit on Time Reversal Violation by at least one order of magnitude.

To develop the experimental activity, a dedicated interaction point including a polarized internal target and a vertex silicon detector, acting as a beam and target polarimeter, have been realized. In addition, a dedicated solenoid (*Siberian snake*) and a sensitive beam-current monitor have already been installed in the ring.

An introduction to the physics case for longitudinal spin filtering and a time-reversal invariance test are introduced in "Methods" section. A brief description of the COSY ring is given in "COSY accelerator and storage ring" section while the experimental equipment to be employed in these investigations and the developed tools are presented in "Experimental setup" to "Silicon detector for beam and target polarimetry" sections. The polarized internal target is described in "Polarized internal target" section, the beam diagnostics and polarization handling in "Beam diagnostics and polarization handling" section, and the Siberian snake in "Siberian snake for the longitudinal spin-filtering test" section. Particular emphasis is given to the detailed description of the silicon vertex detector in "Silicon detector for beam and target polarimetry" section. Results of the commissioning effort are presented in "Commissioning results" section, and the conclusions in "Conclusions" section.

Methods

Longitudinal spin-filtering of a stored proton beam

An intense beam of polarized antiprotons will open new experimental opportunities to investigate the structure of the nucleon [3]. Although a number of methods to provide polarized antiproton beams have been proposed [6–8], no polarized antiproton beams have been produced so far, with the exception of a low-intensity and low-quality, secondary beam from the decay of anti-hyperons that has been realized at Fermilab [9]. Since many years, the PAX collaboration is investigating possible mechanisms to produce such a beam. After having shown the non-applicability of spin-flip to polarize a stored beam *in situ* [10], the collaboration has successfully performed a spin-filtering test on protons with a transversely polarized hydrogen gas target [4].

Spin-filtering exploits the spin-dependence of the strong interaction using a polarized internal target. Since the total cross-section is different for parallel and antiparallel orientations of the spins of the beam and target protons, one spin orientation of the beam particles is depleted at a higher rate than the other and the circulating beam becomes increasingly polarized, while the beam intensity decreases with time (see Fig. 1).

The measurement already performed at COSY constitutes a determination of the transverse spin-dependent polarization build-up cross section. PAX intends to transfer this method to longitudinal polarization to measure the complete spin-dependent cross section as described by the equation

$$\sigma_{\mathrm{tot}} = \sigma_0 + \sigma_1(P \cdot Q) + \sigma_2(P \cdot k)(Q \cdot k)\,, \tag{1}$$

where σ_0 denotes the total spin-independent hadronic cross section, σ_1 the spin-dependent cross section for transverse orientation of beam (P) and target polarisations

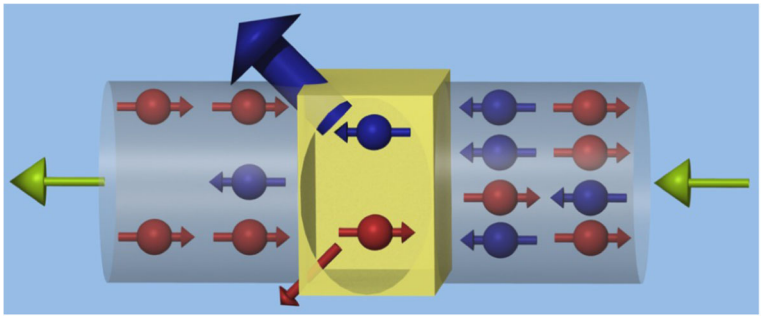

Fig. 1 Spin-filtering concept. The spin-dependence of the hadronic interaction cause a selective discard of one spin state of the stored particles

(Q), σ_2 denotes the spin-dependent cross section for longitudinal orientation of beam and target polarisations, and k the beam direction (notation according to [11]).

The motivation for the longitudinal filtering measurement is the fact that different theoretical models for spin-filtering with antiprotons predict a significantly higher degree of polarization for the longitudinal case than for the transverse one. While for spin filtering with protons, this is not to be expected, the optimization of the polarization buildup with antiprotons requires longitudinal spin-filtering as a necessary step. Once stored antiproton beams become available at FAIR, the collaboration would like to carry out the corresponding spin-filtering experiments to determine the unknown spin-dependent total cross sections σ_1 and σ_2 in double-polarized $\bar{p}p$ scattering.

Experimental approach

The preferred direction of the polarization in a magnetic storage ring is vertical with respect to the beam momentum; longitudinal polarization requires the introduction in the ring of a dedicated solenoid, a so-called *Siberian snake*, by means of which the spin-closed orbit at the target is oriented along the longitudinal direction. Such a snake has been installed at COSY in 2017 in the opposite straight section with respect to the PAX target installation and is ready for operation [12].

A conceptual scheme of a typical polarization buildup measurement cycle is shown in Fig. 2. Spin-filtering and polarization measurement interval will be alternated to monitor the polarization buildup.

The beam polarization will be determined by making use of the beam correlation parameter $C_{z,z}$ of the longitudinal spin-dependent p-p cross section:

$$\frac{\mathrm{d}\sigma}{\mathrm{d}\Omega} = \frac{\mathrm{d}\sigma}{\mathrm{d}\Omega_0} \cdot \left(1 + C_{z,z} P_z Q_z\right) , \tag{2}$$

According to Eq. 2, the beam polarization can be measured by detecting the difference in the detector rates induced by reversing the direction of the target or beam polarization. As the polarization measurement requires the reversal of target or beam polarization, therefore stopping the polarization buildup process itself, the time intervals have to be properly optimized.

The energy dependence of the longitudinal cross section favours the performance of the test at the maximal possible energy in the ring, where electron cooling is still possible. The experiment will therefore be performed at a proton beam energy of $T_p = 135$ MeV.

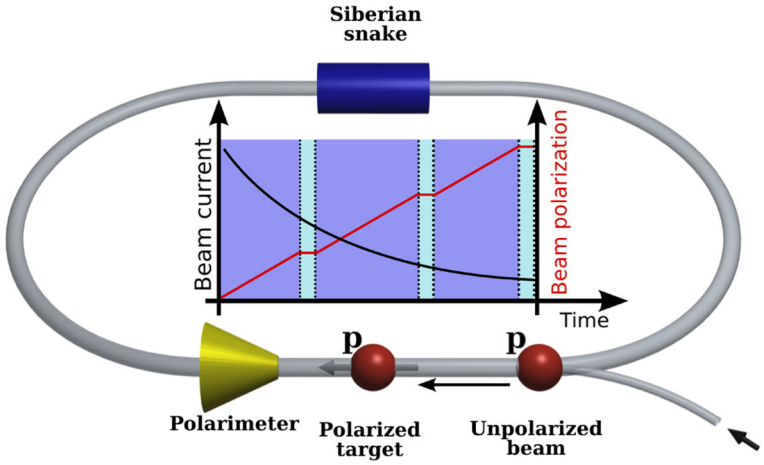

Fig. 2 Cycle scenario for longitudinal spin-filtering. The time intervals of spin-filtering (light-blue) alternate with other where the beam polarization is measured by reversing the longitudinal target polarization (magenta)

Test of time reversal invariance

In contrast to the search for Electric Dipole Moments (EDM) [2], the existence of which would be a manifestation of the violation of *parity* (P) and *time reversal* (T) symmetries, the time reversal invariance test proposed at COSY (TIVOLI[2] experiment) seeks to find evidence for an interaction that breaks time reversal, but conserves parity [13].

Time reversal violating and parity conserving pure hadronic interactions as a source of *CP*-violation in kaon decays was postulated in 1965 by Okun [14], Prentki and Veltman [15], and Lee and Wolfenstein [16]. The term milli-strong *CP*-violation (MSCPV) has been coined for such interactions, and as far as *CP*-violations in weak decays are concerned, predictions from MSCPV would be similar to those from the Kobayashi-Maskawa mechanism adopted in the Standard gauge Model (SM) of weak interactions. While in the SM the *CP*-violation is confined to flavor changing transitions, MSCPV is flavor conserving. Henceforth it predicts time-reversal violation in a much broader variety of processes, including nuclear and strong interactions, nuclear β decays, and T-violating mixing of multipoles in nuclear γ transitions [17].

Based on *CP*-violation in kaon decays and dimensional analysis, the strength of MSCPV can be estimated to be about 10^{-3}. MSCPV predicts neutron EDMs of $d \approx 10^{-24} e.cm$ [17], about seven orders in magnitude larger than the SM prediction. Parity-conserving MSCPV has symmetry properties distinct from that of the QCD θ-term and can not be incorporated into the SM. An intriguing open issue is whether MSCPV can be associated to *CP*-violation beyond the SM, called upon by the large unexplained baryon asymmetry of the Universe [18].

For the TIVOLI experiment at COSY, there is in fact one observable available, namely the total spin-correlation parameter $A_{y,xz}$ in proton-deuteron scattering with polarized beam and target, that would vanish in the absence of some T-odd P-even interaction [19].

[2]Time Invariance ViOLating Interactions

By the generalized optical theorem, the imaginary part of the forward p-d elastic scattering amplitude with these spin orientations is linked to the integral cross section of the corresponding double polarized p-d interaction. At COSY this could be studied by arranging the proton beam polarization along the perpendicular direction with respect to the ring plane while keeping the tensor polarization of the deuteron in the (horizontal) ring plane at an angle of 45° (in the c.m. frame) between the beam and the radial direction.

The principle of the experiment is illustrated in the c.m. frame in Fig. 3, where it is shown that the combined application of the time-reversal and rotation operators leads to the same initial configuration, but with signs of the polarizations of either the proton or deuteron being reversed. Time-reversal invariance therefore means that the total cross section measured with configuration (c) or (d) should be identical to that obtained using (a). The ability to invert either of these polarizations allows a useful check of the systematics of the experiment.

The measurement of such a $\vec{p}\vec{d}$ total cross section in a transmission experiment with an external beam is much less efficient with respect to a storage ring, given the loss in statistics in a single pass configuration. In addition, in a storage ring, one can measure the total cross section simply by measuring the lifetime of the beam as it passes through the target [20–22].

Experimental approach

In principle the TIVOLI measurement of $A_{y,xz}$ could be undertaken at any proton beam energy, but there are good arguments for choosing $T_p = 135$ MeV. It was actually predicted [23] that the sensitivity to T-violating forces should be maximal for T_p of the order of 125 MeV. On the practical side, high-quality polarimetry data for proton-deuteron

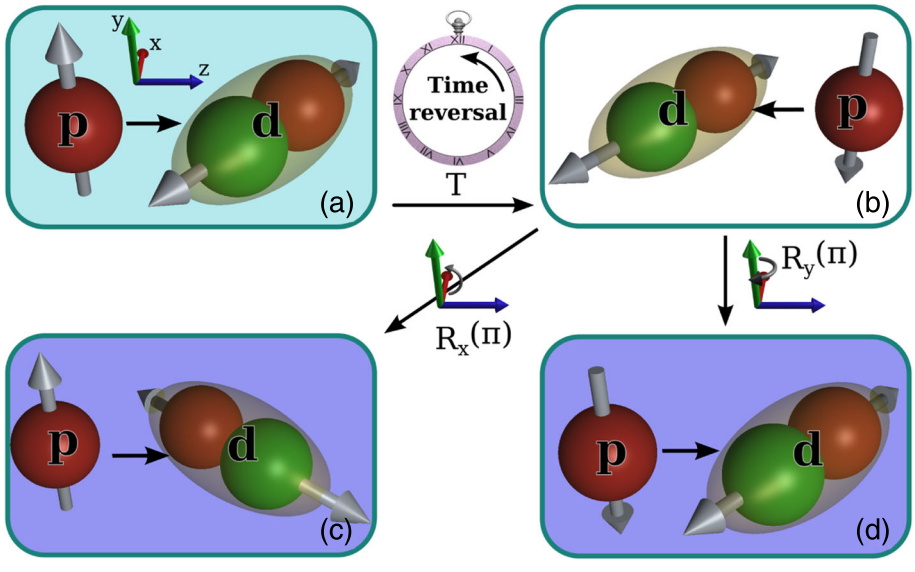

Fig. 3 In-principle demonstration that a time-reversed situation is prepared by either a proton or a deuteron spin-flip. **a** The basic system is shown. **b** The time reversal operation is applied (momenta and spins are reversed and the particles are exchanged). In order to have a direct comparison between situation (**a**) and (**b**), two rotations $R_y(\pi)$ or $R_x(\pi)$ by 180° about the y- or x- axis are applied, leading to the situations (**c**) and (**d**), respectively. This is allowed, since the time reversal operation is invariant under rotations

elastic scattering are available at 135 MeV [24]. In addition, at this energy the electron cooler can continuously cool the COSY beam over the complete cycle of measurements. It should also be noted that only one depolarizing resonance has to be crossed to arrive at this energy.

The TIVOLI experiment could be carried out at the PAX internal target station. Using the new high precision beam current measurement system, COSY will serve as accelerator, storage ring, and ideal zero-degree spectrometer and detector for the TIVOLI experiment.

The experiment is planned as a null transmission experiment in the storage ring using the T-violation sensitive observable $A_{y,xz}$ available in double-polarised pd scattering. A polarised proton beam, together with a tensor polarised deuterium gas target located the PAX interaction point, will be used for the experiment. The $A_{y,xz}$ observable will be determined from the difference of beam lifetimes measured for two independent beam-target spin polarisation states (see Fig. 4).

For this reason, the experiment puts stringent requirements on the precision of beam lifetime determination and consequently the resolution of the beam current measurement device. A resolution of $\Delta I/I = 10^{-4}$ integrated over one second of beam current measurement will allow us to improve the present upper limit on the T-violation by an order of magnitude in one month of measurement time [25].

COSY accelerator and storage ring

The COoler SYnchrotron and storage ring COSY accelerates and stores unpolarized and polarized proton or deuteron beams in the momentum range between 0.3 GeV/c and 3.65 GeV/c. COSY has a racetrack design with two 180° arc sections connected by 40 m long straight sections. It is operated as a cooler storage ring with internal targets or with an extracted beam. Beam cooling, i.e., reducing the momentum spread of the beam and shrinking the transverse equilibrium phase space, is realized by electron cooling up to proton-beam momenta of 0.6 GeV/c and by stochastic cooling for proton

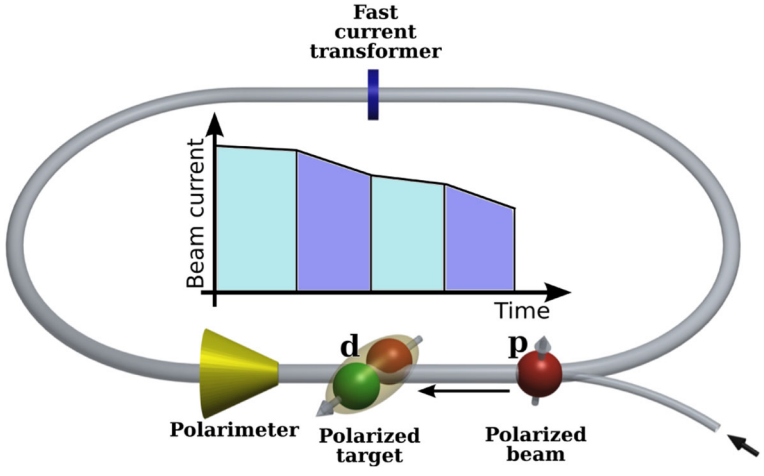

Fig. 4 Main components of the experimental setup for the TIVOLI experiment: polarized beam from the injector cyclotron, polarized deuteron target from an ABS, polarimeter and beam current sensor. Time reversal invariance will be accessed by detecting the difference in the beam lifetime between the situation a) and c) or d), depicted in Fig. 3, as schematically indicated in the inset

momenta above 1.5 GeV/c. Polarized proton and deuteron beams are routinely delivered to experiments over the whole momentum range. Polarized beams from the ion source are preaccelerated in the cyclotron JULIC, injected and accelerated in COSY without significant loss of polarization. Imperfection and intrinsic depolarization resonances are overcome by well-established procedures (for additional details on the COSY storage ring see [12] and included references). A schematic representation of the COSY storage ring is presented in Fig. 5. The arrows indicate the position experimental setups described in the paper.

Low-β section

In order to implement the low-β section required by the PAX experiment, four quadrupoles from the decommissioned CELSIUS ring were installed in one of the COSY straight sections. Switching on the new PAX quadrupoles required only minor modifications of the standard COSY operation settings at injection energy. The commissioning has shown that the PAX optics caused neither additional acceptance restriction nor shorter lifetimes. A measurement of the β-functions at the positions of the new quadrupoles coincides well with the calculated values of about 0.3 m at the center of the target. Additional technical details of the low-β section and its commissioning are presented in [12].

Experimental setup

In the next sections, the different components and developed tools of the experimental setup are presented. A schematic view of the overall interaction point is shown in Fig. 6 and consists of:

- the polarized internal target ("Polarized internal target" section);
- beam diagnostic and polarization handling ("Beam diagnostics and polarization handling" section);
- siberian snake ("Siberian snake for the longitudinal spin-filtering test" section);
- silicon detector for target and beam polarimetry ("Silicon detector for beam and target polarimetry" section).

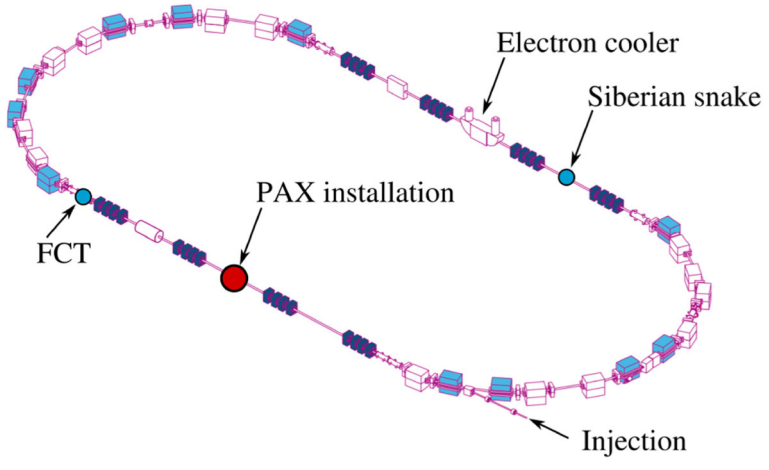

Fig. 5 Schematic picture of the storage ring at the Forschungszentrum Jülich evidencing the location of various components of the experimental setup. The Fast Current Transformer (FCT) is described later in the text

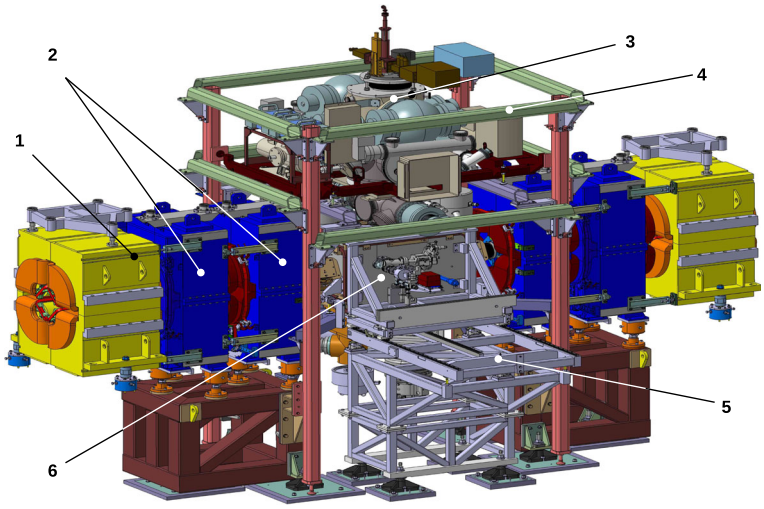

Fig. 6 View of the PAX installation at COSY from the interior of the ring (the beam comes from the left). 1: COSY quadrupole magnet; 2: two of the four PAX quadrupoles forming the low-β insertion by doublet focusing (DF-FD); 3: atomic beam source (ABS); 4: support system; 5: flange supporting rail system; 6: PAX target chamber housing the detector and the storage cell. The Breit-Rabi polarimeter (BRP) and the target-gas analyzer (TGA) are mounted towards the outside of the ring. (Figure taken from Ref. [12].)

Polarized internal target

The polarized hydrogen and deuterium target was moved from HERMES-DESY [26] to Jülich in 2006. Before re-using the system at COSY, the pumping system, data acquisition, and control electronics have been completely renovated. In addition an openable storage cell has been developed. The use of an openable storage cell provides no limitation of the ring acceptance and can be tolerated at injection of the uncooled beam into the ring. The cell is opened at beam injection and closed after the beam has been cooled and its emittance and size are reduced. The cell design is described later in this paper in the section presenting the silicon detector.

The PAX target is composed of a Polarized Atomic Beam Source (ABS), a Breit-Rabi polarimeter (BRP) and the mentioned storage cell. The ABS injects polarized hydrogen atoms into the cell, while the BRP measures the polarization of an effusive beam extracted from the cell. A schematic view of the components is shown in Fig. 7. Target areal densities of 5×10^{13}atoms$/cm^2$ are achieved by injecting nuclear spin polarized hydrogen or deuterium atoms produced by the ABS into a storage cell (see "Openable storage cell" section). Further details about the design and performance of the target can be found in [27].

Dual rf cavity for hydrogen and deuterium

The foreseen experimental activity requires to run the target both with hydrogen (H) and deuterium (D) atoms. In order to switch from H to D or vice versa, the resonating structures of the source and polarimeter have to be exchanged and up to now, a tedious fine-tuning of the transition unit was required.

Therefore, a system of RF-resonators has been developed that can operate on the frequencies required for H or D beams *without* mechanical changes. In addition, the magnetic component of the RF-field should be tilted by 45° with respect to the static field in order to allow for both σ and π transitions ($\Delta m_F = 0$ and ± 1, respectively). Such a *Dual*

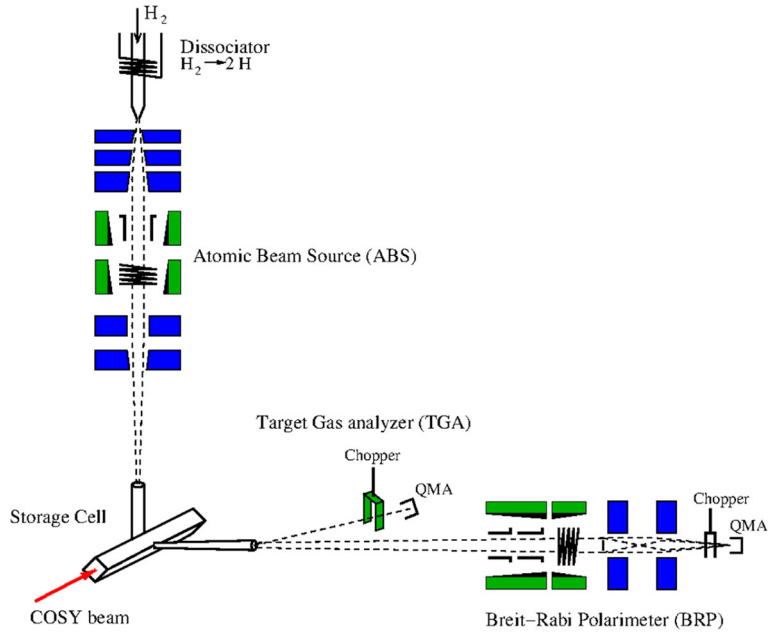

Fig. 7 Schematic drawing of the PAX polarized target with the ABS in the vertical position, the storage cell on the ring axis, and the target diagnostic system in the horizontal position. The Target Gas Analyzer (TGA) determines the atomic to molecular fraction of the effusive beam from the storage cell, while the Breit–Rabi Polarimeter (BRP) measures the degree of polarization of the atomic sample

Cavity has been developed and implemented in the polarized source capable of serving both H and D beams [28] (see Fig. 8).

Holding field and pumping system

To define the target gas polarization direction, the PAX target chamber hosting the storage cell has been equipped with three sets of Helmholtz coils providing magnetic holding fields in x, y and z direction. For reasons of space optimization and functionality, the coils have been mounted on the edges of the chamber (see Fig. 6 of Ref. [12]).

A NEG pumping system, designed and constructed in the FZJ-ZEA mechanical workshop, has been installed below the PAX target. The pump consists of a battery of 10 NEG cartridges. During the activation of the cartridges at 450°C, a mechanical shutter separating the pump from the chamber is closed. In this way, the temperature in the target chamber is limited to less than 80°C. By means of a calibrated H_2 gas inlet a pumping of $S = 12000l/s$ has been measured. The use of the getter pump during COSY operation allows the achievement of a target chamber pressure in the 10^{-10} mbar range without gas load from the ABS and in the low 10^{-8} mbar range with H gas injected from the ABS in one hyperfine state (3×10^{16}atoms/s).

Beam diagnostics and polarization handling

Precise fast current transformer for TIVOLI

The Time Reversal Invariance test at COSY requires the precise determination of the beam lifetime. For this reason, a high resolution bunched-beam current measurement system based on a Fast Current Transformer (FCT) and Lock-In Amplifier (LIA) has been built.

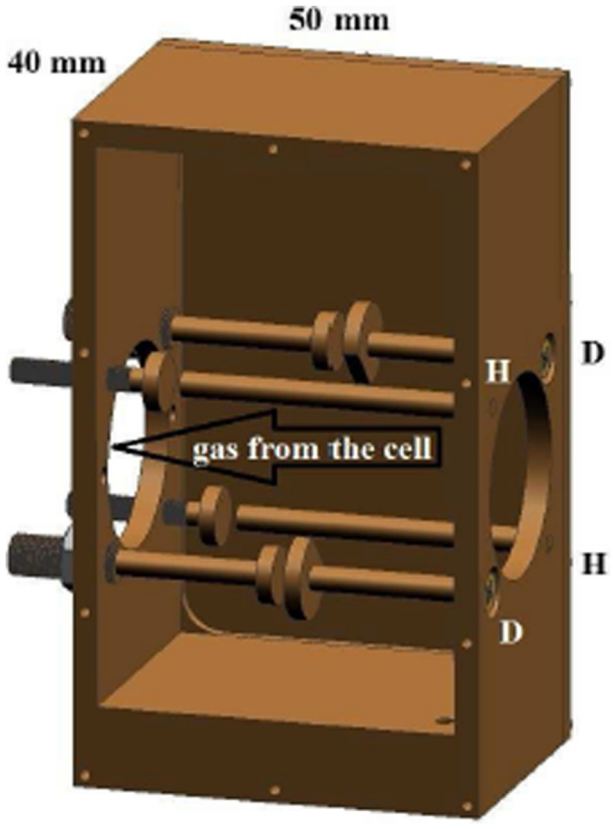

Fig. 8 The SFT H-D dual cavity [28]. Coupled rods for H and D are tilted by 45° with respect to the homogeneous and gradient fields

Tests showed that it is not possible to reach a resolution better than 10^{-3} in the current measurement of a coasting beam based on the conventional DC Beam Current Transformers. It was therefore decided to make use of inductive or capacitive pick-ups [29, 30] in order to obtain a better sensitivity and resolution for the average bunched beam current measurement. In particular, a new high resolution beam current measurement system was developed using an *inductive* sensor sensitive to bunched beam.

A Fast Current Transformer (FCT) has been obtained from Bergoz Instrumentation[3]. The sensor has been mounted on a UHV-compatible flange together with a calibration winding. The FCT as installed in one of the straight section of the COSY ring is shown in the left panel of Fig. 9. The detector occupies less than 10 cm of space in the ring [31].

To cope with the low beam intensity in COSY, the device has been equipped with a custom-built low noise preamplifier. The calibration winding has been connected to a precision current source allowing for calibration of the FCT during normal COSY operation.

[3]Bergoz Instrumentation http://www.bergoz.com/en/fct

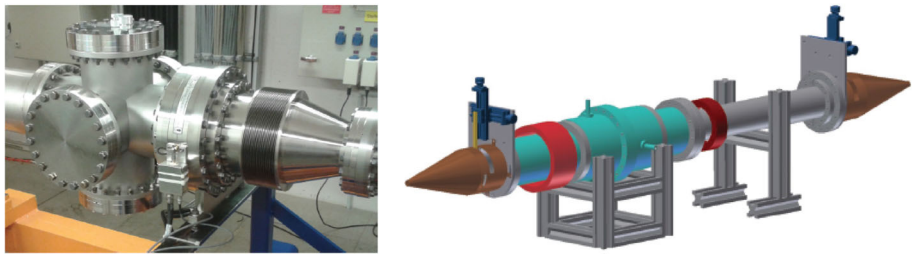

Fig. 9 Left: Fast Current Transformer from Bergoz Instrumentation installed at COSY. The FCT in the ring is equipped with a custom build preamplifier and a current source for calibration. Right: The test station for the beam current measurement devices. Different beam current sensors can be implemented into the test stand. The wire inside the tube is moved using XY tables (blue) mounted on both sides of the system. The wire tension system is covered inside the tapers (copper colored)

Test at COSY

The scheme of the FCT measurement system prepared for COSY is presented in Fig. 9. The preamplifier and current source are connected to the FCT installed in the COSY tunnel. The amplified signal is transferred over a coaxial cable to the measurement setup inside the COSY hall. The signal is split between a Lock-In Amplifier, readout via Ethernet, and a main amplifier that distributes the signal to other users.

The calibration module provides a high precision rectangular voltage signal to the current source connected to a calibration winding of the FCT. The first measurements done at COSY confirmed the extremely good sensitivity of the FCT from Bergoz Instrumentation. At first, the bunched beam intensity in the ring was calibrated using a standard COSY beam-current transformer and later the beam intensity was reduced by readjusting the injection beam line. Beam currents in the range from 2×10^9 down to 4×10^4protons in the ring have been detected by the new FCT.

Additional tests

To perform a detailed study of the FCT performance, a second system, analogous to the one used at COSY, has been set up in the laboratory (see Fig. 9, right panel). In the test stand the beam signal was induced by an Arbitrary Waveform Generator controlled by the DAQ. The signal in the wire is monitored using a receiver device on the other side of the test stand. In the laboratory, the trigger module, controlled over the network, generates all the necessary hardware trigger signals for the readout system.

A resolution of $\Delta I/I = 1.9 \times 10^{-4}$ for an average beam current of 1 mA has been reached in the laboratory. An order of magnitude better resolution can in principle be reached when the temperature variations of the system are reduced.

Siberian snake for the longitudinal spin-filtering test

Basic snake parameters

Siberian snakes are used to avoid crossing depolarizing resonances in circular accelerators. The spin rotation in a full Siberian snake is 180° per turn around the beam axis, forcing the spin tune to be a half integer, independently of the beam energy [32]. If only one Siberian snake is used, the invariant spin axis is in the horizontal plane. This is an interesting feature to deliver longitudinally polarized beam to internal experiments.

To realize a full Siberian snake an integrated magnetic field of 3.42 Tm at 911.86 MeV/c has to be provided by the solenoid. Superconducting magnet technology was used to achieve an acceptable length of the snake [33]. A dedicated solenoid has been designed and constructed by Cryogenics[4], its main technical data are summarized in Table 1.

The snake was delivered to Jülich in 2017 and was successfully tested in the laboratory before the installation into COSY. The sequence shown in the left panel of Fig. 10 has been performed with a ramp speed of 0.76 A/s to a maximum field of 5 T and 300 s hold time in between. The temperatures in the various subsystems stayed below 5.5 K during the ramp procedure.

Snake commissioning

To ensure that the beam polarization is oriented in the longitudinal direction in the straight section where the PAX interaction point is located, the superconducting solenoid has been installed in the opposite straight section of the ring (see right panel of Fig. 10). In preparation of the longitudinal spin-filtering test, a commissioning of the Siberian snake with beam at COSY is foreseen.

For this experiment the proton beam with vertical polarization will be injected into COSY, electron-cooled and accelerated to beam momenta between 520 and 920 MeV/c. The momentum range for commissioning is chosen in a way that the solenoid can be operated as a full Siberian snake. By ramping the solenoid from zero to 1.95 and 3.4 Tm, respectively for the two momenta, the vertical beam polarization will be transferred into the horizontal plane. The beam will in particular be longitudinally polarized in the straight section where the PAX installation is located. The PAX detector will be used to measure the change of vertical beam polarization when the snake is ramped.

Silicon detector for beam and target polarimetry

In order to cope with the foreseen experimental activities, a silicon vertex detector has been realized to serve as a beam and target polarimeter in proton-(anti)proton and proton-deuteron internal gas target experiments in the 30 MeV to 200 MeV beam energy range. All the components have been selected to be high-vacuum compatible and the detector has been tested to operate at pressures in the 10^{-9} mbar range.

The detector is composed of four identical quadrants combined in a diamond-shaped configuration. It hosts a storage cell where polarized or unpolarized H or D target atoms

Table 1 Dimensions and characteristics of the Siberian snake at COSY

Length of the cryostat	975 mm
Bore diameter	90 mm
Minimum field integral along axis	4.7 Tm
Maximum field	6 T at 258.83 A
Cooling liquid	Helium, cryogen-free operation

[4]Cryogenics Ltd. UK http://www.cryogenic.co.uk

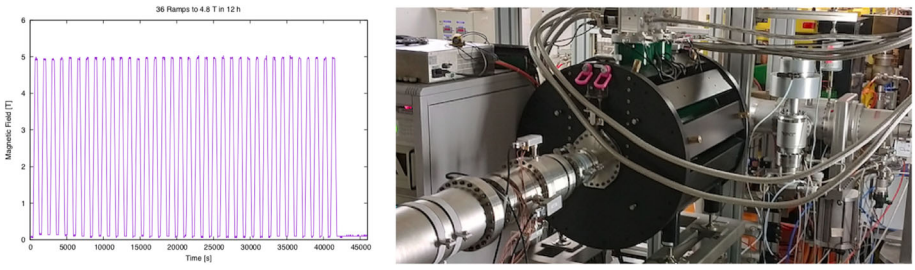

Fig. 10 Left: Sequence of ramps to 5 T at a ramp rate of 0.76 T/s measured with a hall probe. Right: A picture of the Siberian snake installed inside COSY (see also Table 1)

and molecules can be injected. A picture of the detector is shown in Fig. 11, while the schematic side and front views with overall dimensions are depicted in Fig. 12.

Each quadrant consists of three layers of double-sided silicon-strip sensors mounted inside an aluminum box and their relative front-end readout system. Sensors and readout electronics are cooled by separate circuits. The modularity allows to independently test each quadrant and its associated electronics and to rapidly replace it in case of malfunctions.

The first detector layer consists of two silicon sensors type TTT1 by the company Micron[5], which were recovered from the recoil detector of the HERMES experiment [26], and mounted side by side on a common ceramic frame. The detectors are 300 μm thick and have an active area of 97.3 mm × 97.3 mm. The electrical contacts are structured with 128 strips (strip width 702 μm, pitch 758 μm).

Before assembly inside the quadrant housing boxes, the ceramic frames have been mounted on an aluminum frame and the strips have been ultrasonically bonded to the kapton foils that connect the detectors to the supply voltage and to a charge-sensitive preamplifier.

The second detector layer is composed of two silicon detectors of type TTT2, also from Micron. For this case, the sensors are individually mounted on the ceramic frame. These detectors are 300 μm thick and present an active area of 97.22 mm × 97.22 mm. The contacts are structured with 128 stripes (strip width 700μm, *pitch*760μm). The strips are bonded to kapton films glued to the ceramic frames. The two detectors are then mounted side by side on an aluminum frame, as shown in Fig. 13.

The third layer is realized with a single silicon sensor. It is also a TTT2 detector from Micron, with a thickness of 1000 μm. The aim of the layer is to increase the stopping power and to extend the detector applicability to the possible identification of deuteron-breakup events in the low energy domain.

Openable storage cell

An openable storage cell has been realized in the INFN-Ferrara mechanical workshop (see Fig. 14). The cell allows to increase the target density by two orders of magnitude. The use of an openable storage cell is a highly desirable feature for an internal target experiment. The cell is opened at beam injection increasing the accelerator acceptance

[5]Micron Semiconductor Ltd, http://www.micronsemiconductor.co.uk

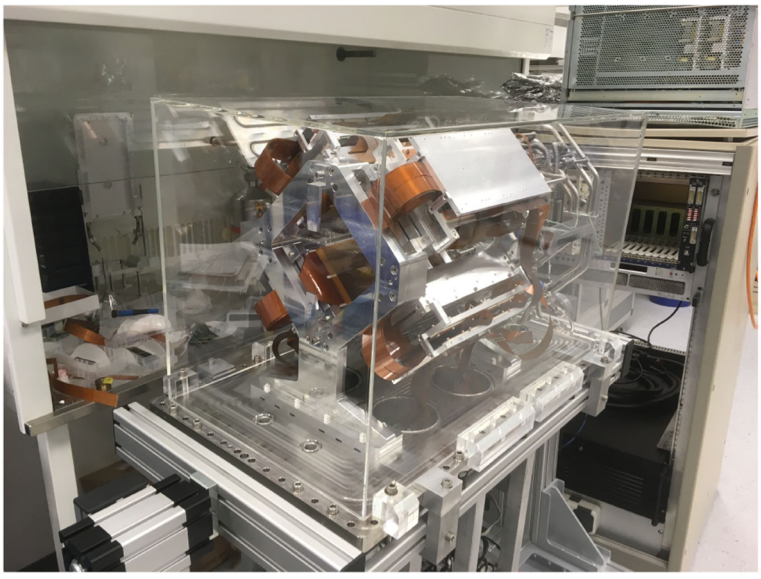

Fig. 11 Photograph of the PAX multipurpose detector

and closed after the beam has been cooled and its emittance and size are consequently reduced.

The cell itself is 40 cm long and has an internal diameter of 10 mm when closed. It has been realized with an aluminum foil of 50 μm thickness. Polarized gas can be injected into the cell through a tube installed in the upper part of the cell [34]. A sample of the target gas diffuses through a side tube into a diagnose system that measures the atomic polarization (Breit-Rabi polarimeter [35]) and the atomic fraction (Target Gas Analyzer [36]).

A dedicated insertion mechanism allows for replacement of the cell without interference with the detector. The assembly of the four quadrants and the cell is accomplished by using a dedicated motor driven rotatable support structure on which the detector flange is mounted.

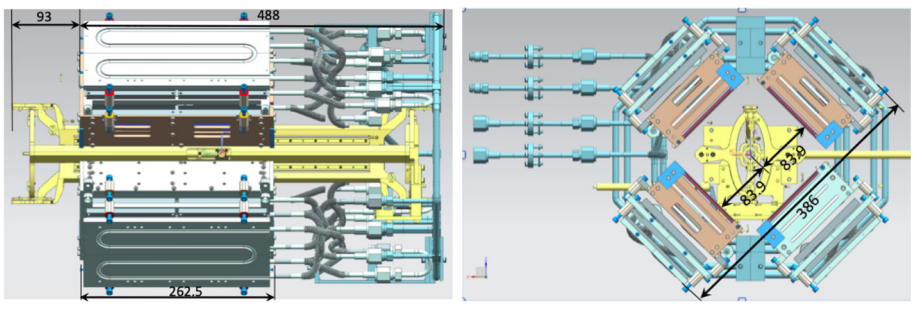

Fig. 12 Side and front views of the PAX detector. The blue connections show the pipes of the cooling circuits; the aluminum box containing the sensors are shown in brown; the storage cell and its support structure are in yellow

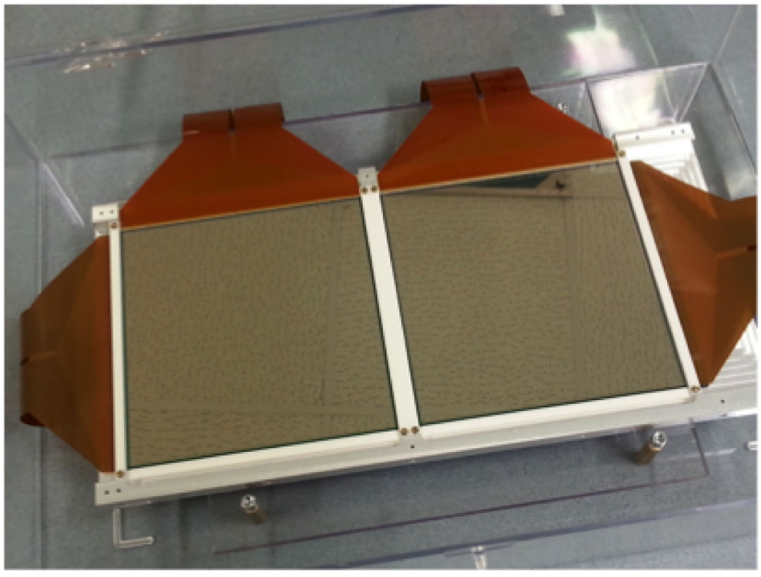

Fig. 13 Second layer of the detector with the TTT2 300 μm thick sensors

Cooling and vacuum

Cooling of the detectors is provided by two independent circuits, operated by LAUDA[6] cooling modules, allowing to set different working temperatures for the silicon sensors and the readout boards (see Fig. 12). The estimated total heat produced by the electronic readout boards amounts to about 15 W per quadrant. During operation, the temperature of both sensors and electronics reached about $5°C$. All components of the detector have been selected to be high-vacuum compatible. Before installation inside the COSY ring for the commissioning work, the completely assembled detector has been tested to reach a pressure in the 10^{-9} mbar range.

Electronic readout

The readout electronics is based on a scheme that has been developed for the ANKE spectrometer. The in-vacuum board carries the readout chips with 11 MeV linear range, and a time resolution of better than 1 ns, sufficient to provide a fast signal for triggering. The interface card outside the vacuum provides power supplies, control signals, trigger pattern threshold and calibration pulse amplitudes to the front-end chips. The vertex readout module developed at Jülich comprises a sequencer together with a 12 bit ADC with 10 MHz sampling; it allows common-mode correction for hardware zero-suppression to reduce the output flow to 0.1 MByte/s with less than 50 μs dead time. A programmable trigger and a pre-scaler module have been developed to provide a flexible trigger logic.

Preamplifier board

The front-end preamplifier boards employ VA32TA2 integrated circuits by the company IDEAS[7]. This choice allowed us to make partial re-use of the hardware and software already developed for the readout of the silicon telescopes of the ANKE experiment [37].

[6] LAUDA Heating and Cooling Systems, https://www.lauda.de/en/individual-temperature-control-systems/industrial-heating-and-cooling-systems.html
[7] Integrated Detector Electronics AS, https://ideas.no.

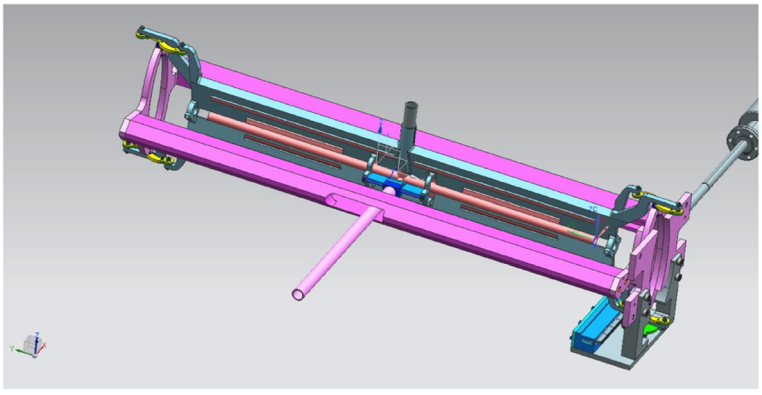

Fig. 14 Storage cell in the closed position. The polarized atomic beam is injected into the cell through a tube in the upper part of the cell (blue color), while a sample of the target gas diffuses into the direction of the BRP system through a side tube (pink color)

A VA32TA2 chip consists of 32 identical channels, each routing the "IN" signal from the silicon detectors through a preamplifier and then through the "VA" and the "TA" branches to obtain the charge amplitude and the timing and trigger informations, respectively.

In order to adapt the chips to the different thicknesses of the used silicon sensors (300 μm and 1000 μm), two kinds of PCBs have been realized. In particular, a charge divider circuit has been realized that enhances the energy dynamic range of the readout system by a factor 2 (see Fig. 15).

The VA32TA2 chips are bonded to the carrier PCB and then encapsulated in a two-step process: first a "dam" (inset in Fig. 15) of EPO-TEK H70E-2 epoxy is created and cured and then the dam is filled with EPO-TEK 509FM-1-LB epoxy which also is subject to curing. The ROGER 3003 insulating material is used in the front end PCBs for its favourable outgassing properties. The specified PCB thickness was 30 mil (0.8 mm).

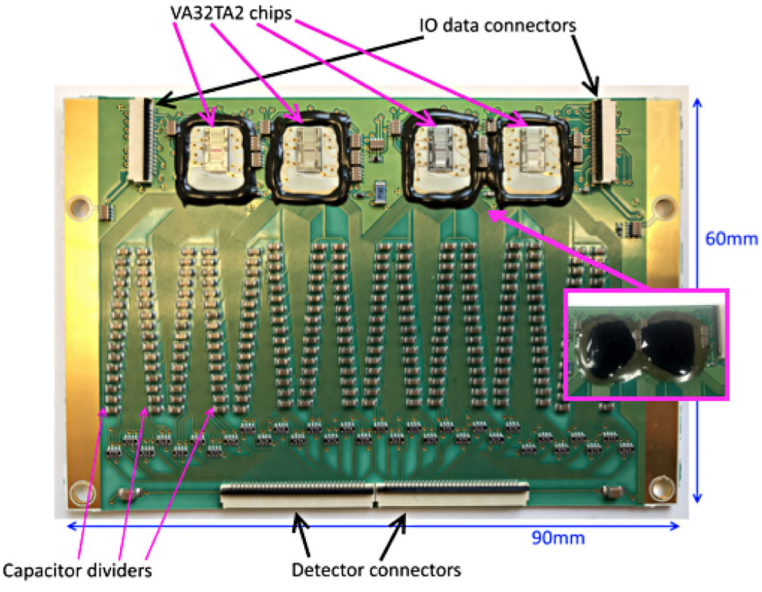

Fig. 15 Front-end PCB with VATA chips; in the inset, the epoxy protection layer is shown

Low voltage and high voltage supply for the sensors and the chips are provided by the MPOD crate by Wiener[8], that can host both HV and LV supply generator modules.

Repeater card

To control the front-end PCBs and to re-condition the analog signal transported by long capton cables, repeater cards have been developed and installed on the outer part of the detector flange (Fig. 16). The functions supplied by the cards are:

- initialization of the chips for data taking;
- amplification of the analog signals from the front-end chips and transmission to the DAQ system;
- adaptation of the trigger signal from the chips and transmission to the trigger system.

Vertex ADC

The analogue to digital converter module (Vertex ADC) has been designed and realized by the Zentralinstitut für Systeme der Elektronik (ZEA-2) of the Forschungszentrum Jülich (Fig. 17). Each module is designed to read both sides of one silicon sensor. One board can read a maximum of 1024 channels. The chips are configured via a serial bus. On the bus, five trigger lines are available. In the FPGA two completely separated programmable sequencers for the VA timing are available. Each channel presents three independent and completely separated addressable memory areas. The blocks are used to store sequences and parameters for the needs of Common Mode. The connection to the LVDS bus is also done via the FPGA.

Trigger

Three types of boards in VME 6U format were developed for the silicon detector's trigger system at Electronic Workshop of INFN-Ferrara,

- the TRIGGER,
- the PRESCALER,
- and the PAX_SPI_BUS DRIVER boards.

The TRIGGER module integrates the functions of a number of delay and logic modules in NIM format by which the trigger system was originally built, with clear advantages in flexibility and reproducibility. The TRIGGER boards receive the VA32TA2's "TA" signals, upon which they perform signal level-translation, de-skewing through programmable delays and combination through a programmable look-up table to generate the TRIGGER signals. These eventually command the start of the sequential readout of the analog information stored on the sample-and-hold circuits of the "VA" branch of the channels of the VA32TA2.

The VME 6U TRIGGER board is shown in Fig. 18 and features eight inputs for the VA32TA2's fast trigger signals and six additional inputs for gate, veto, strobe and clear signals. The picture shows:

- the DACs that defines the thresholds for the discriminator-shaper circuits used to regenerate the input signals and the programmable pulse generators (PPG), determining the discriminator-shaper's output pulse width;

[8] W-IE-NE-R Power Electronics http://www.wiener-d.com

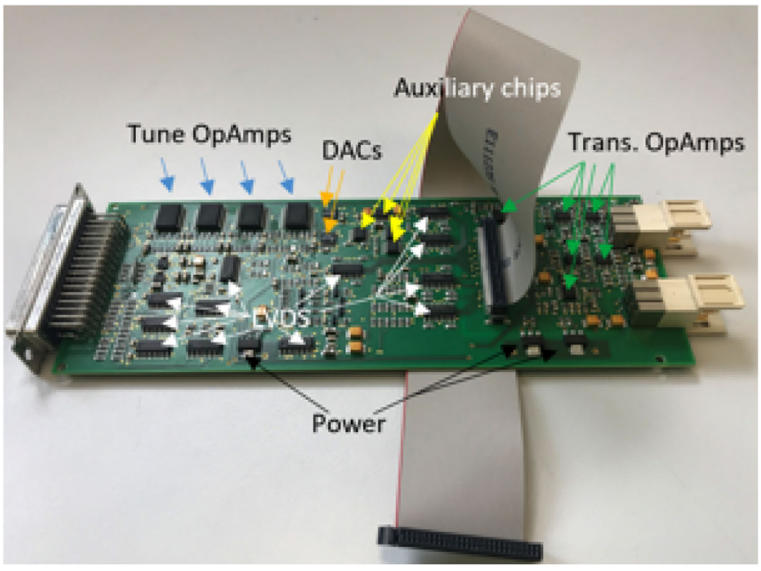

Fig. 16 Repeater card with references to its main components

- the programmable delay lines (PDL) used to de-skew the reshaped trigger pulses prior to their combination through the look-up-tables programmed inside the CPLD (Complex Programmable Logic Device);
- the FPGA which handles the VME and the serial dedicated "PAX_SPI_BUS" interfaces for remote programming of the board features.

A program coded in C^{++} and running on a host computer has been used to access another VME 6U board acting as a controller of the dedicated PAX_SPI_BUS serial communication channel.

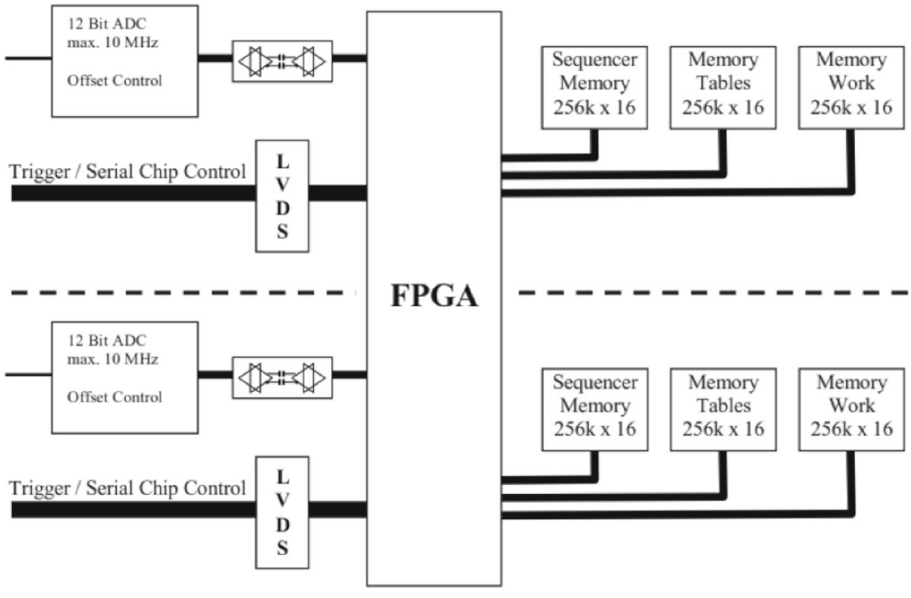

Fig. 17 Diagram of the Vertex ADC

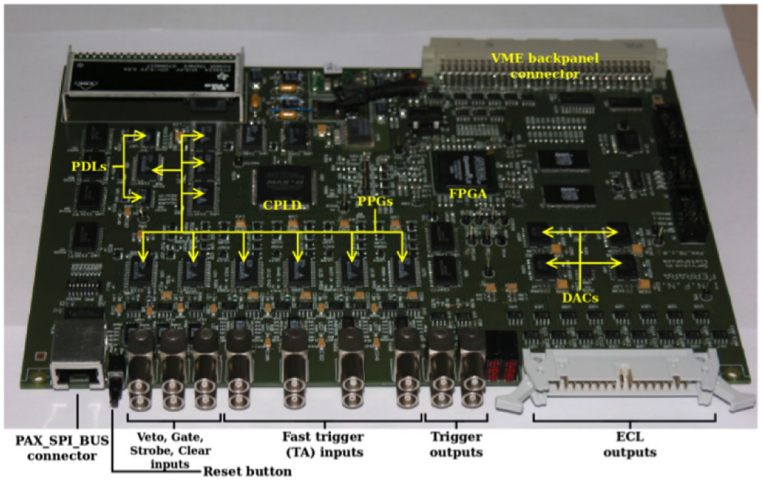

Fig. 18 Trigger module of the PAX detector

The VME 6U PRESCALER module has been designed to receive the outputs of the TRIGGER boards and filter them according to a programmable pre-scaling factor. Care was taken in the design to minimize the skew and jitter introduced by the pre-scaling function on the trigger signals not to compromise on the precision of the start signals to the VA32TA2 readout system and thus the precision of the analog measurements. The PRESCALER card features 16 independent channels accepting NIM-level input and generating NIM-level and ECL-level outputs.

Commissioning

After calibration of the single quadrants and sensors on an external test bench, the assembled detector has been installed for commissioning in the COSY storage ring. The commissioning exploited an unpolarized proton beam at an energy of $T_p = 135$ MeV scattering off a vector polarized deuteron target.

As described in "Silicon detector for beam and target polarimetry" section, each layer of the detector consists of two stripped sensor sides, with strips oriented respectively along the beam axis on one side and orthogonally on the other. Thus, each layer ideally measures a two-dimensional coordinate for each track. The average number of strips in a track hit was about two in the first two layers and four in the third thick layer, and a track coordinate was reconstructed as a weighted average according to the charge distribution in the strips that fired. By extending the straight line of a track to the beam axis, one could find the longitudinal and transverse coordinates of the interaction point with an RMS accuracy of about 2 mm.

The deposited energy loss in the detector was calibrated with the use of a GEANT-based simulation [38]. The left panel of Fig. 19 shows a distribution of the energy deposit in the second layer versus the one in the third layer. One can see the loci of protons and deuterons that were stopped in the third layer and of those that passed it. To avoid thickening of the lines, the plot was obtained in a narrow range of the laboratory polar angle around 70°. Analogous dependencies were observed for the combination of the first and second layers. By comparing such plots derived from the simulation with the correlations of the measured charges, the energy calibration parameters were derived. The left panel

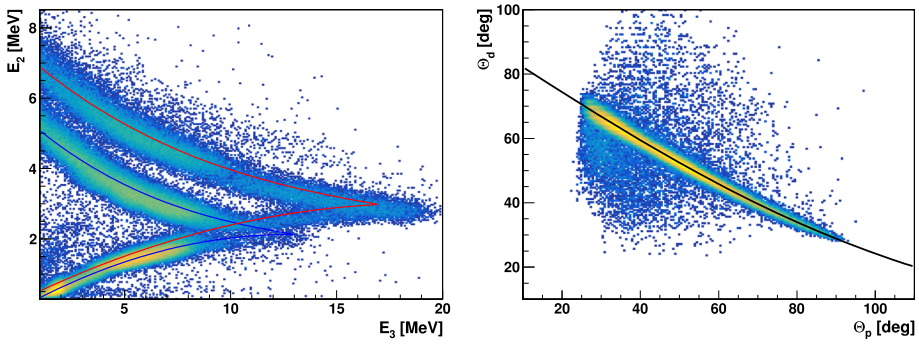

Fig. 19 Left: Energy deposit in the second layer vs. deposit in the third for the tracks with $60° < \theta < 80°$. The two upper bands contain deuterons and protons stopped in the third layer, with the deuteron band above. The lower rising band contains the particles passing through the third layer. The curves represent the energy deposit derived from simulations: red for deuterons, blue for protons. Right: Correlation of laboratory polar angles in two-track events, selected by *pd*-elastic azimuthal correlation. The energy loss cuts are applied to select protons and deuterons passing through the third layer

of Fig. 19 demonstrates also the possibility to identify the particles that are stopped in the second or third layers.

As the beam energy in the experiment was below the pion production threshold of $T_{\text{thresh}} = 207$ MeV, the dominant processes are from *pd* elastic scattering and from deuteron breakup. The former, with both final state particles detected, is also the cleanest one to select, and was primarily used for the detector performance study as well as for the target polarimetry.

The right panel of Fig. 19 shows the polar angle distribution of the identified *pd* elastic events. The events were selected by requiring matching vertex coordinates for the two tracks and proper correlation of the azimuthal angles, the tracks were ordered using their energy loss. Both the final state proton and the deuteron had enough energy to penetrate the third layer when detected in coincidence. Despite the non-ideal vacuum conditions in the target chamber during the beam time (no sensible dependence of the total detector rate could be detected with and without injection of polarized gas into the cell), the *pd* elastic events could be cleanly selected with a background level of only 1.5%.

The detector efficiency was studied by using *pd* elastic scattering as well. For that, a track was reconstructed by using two out of three layers, and the probability to find a hit in the third layer at the position defined by the track was determined. Given the lower multiple scattering compared to deuterons, only the proton tracks were used for this investigation. The energy deposit of the protons amounted to 0.6 MeV in each of the two 300μm thick layers and 2.0 MeV in the 1 mm thick layer. All detectors showed an efficiency above 99%.

Commissioning results

Measurement of the target polarization

In order to determine the target polarization, the direction of the target holding field was regularly alternated between the up and down directions. The differential cross section for the interaction of an unpolarized proton beam impinging on a transversely vector polarized deuterium target is given by

$$\frac{\mathrm{d}\sigma}{\mathrm{d}\Omega}(\theta,\phi) = \frac{\mathrm{d}\sigma_0}{\mathrm{d}\Omega}\left[1 + \frac{3}{2}QA_y^d(\theta)\cos\phi\right], \tag{3}$$

where $\mathrm{d}\sigma_0/\mathrm{d}\Omega$ is the unpolarized cross-section, $A_y^d(\theta)$ is the analyzing power, Q is the target polarization, and θ and ϕ denote the polar and the azimuthal scattering angles, respectively. Accurate *pd* elastic analyzing power data are available exactly at $T_p = 135$ MeV [24].

The target polarization Q has been obtained from the measured asymmetry, using the cross-ratio method [39]. This method provides a cancellation of all first order false asymmetries caused by differences in acceptance and efficiency of the two detectors, and of the integrated luminosity accumulated for the two polarization directions. The cross ratio δ is defined by means of the rates $Y(\theta,\phi)_{\mathrm{L,R},\uparrow,\downarrow}$ detected in the left (L) and right (R) detectors for data samples with spin up ($\uparrow$) and down ($\downarrow$) target polarizations,

$$\delta = \sqrt{\frac{Y_{\mathrm{L},\uparrow}(\theta)\cdot Y_{\mathrm{R},\downarrow}(\theta)}{Y_{\mathrm{L},\downarrow}(\theta)\cdot Y_{\mathrm{R},\uparrow}(\theta)}} = \frac{1+\frac{3}{2}QA_y^d(\theta)}{1-\frac{3}{2}QA_y^d(\theta)}. \tag{4}$$

In this framework, the asymmetry is defined as

$$\varepsilon = \frac{\delta-1}{\delta+1} = \frac{3}{2}QA_y^d\,|\langle\cos\phi\rangle|, \tag{5}$$

where $|\langle\cos\phi\rangle|$ is the trigonometric average over the detector acceptance.

In the left panel of Fig. 20, the observed asymmetry ε (corrected for $|\langle\cos\phi\rangle|$) is presented for the *pd* elastic reaction. The events were selected by the common vertex criterion, *pd* angular correlations and cuts on the energy loss. The remaining low background was accounted for in each θ_p bin in the cm and for each polarization direction. The resulting polarization of

$$\langle Q\rangle = 0.462 \pm 0.010 \tag{6}$$

denotes the total polarization of the target gas averaged over the length of the storage cell.

The dependence of the polarization on the longitudinal coordinate Z of the production point is shown in the right panel of Fig. 20, where the origin corresponds to the cell and detector center. The Z axis points along the beam direction. The histogram values in each bin are obtained in the same way as demonstrated in the left panel of Fig. 20, but for events with Z falling into that bin. The range of Z shown is defined by the detector acceptance for the reaction. One can see that no polarization loss is observed away from the injection tube of the cell located at $Z = 0$.

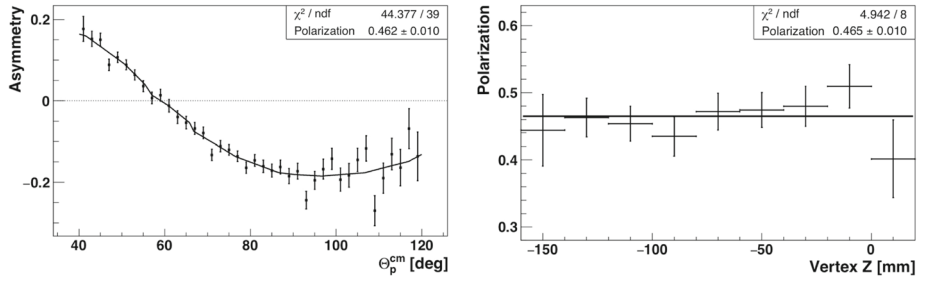

Fig. 20 Left: Experimental asymmetry in *pd* elastic scattering as a function of proton polar angle in the cm. The curve shows interpolated A_y^d data from Ref. [24], scaled to fit our data. Right: Target polarization Q estimated as a function of the longitudinal vertex coordinate Z along the storage cell. The straight line represents a fit with a constant scaled with the sought-for value of the target polarization to fit our data

Discussion

The detector commissioning offers in perspective the chance to validate and to provide an absolute calibration of the target polarization as measured by the Breit-Rabi polarimeter (BRP). The BRP acts as a sampling polarimeter and measures the polarization of a sample of the target gas diffusing out from the center of the storage cell. It has an intrinsic systematic limitation related to the representativeness of the measured sample polarization of the average polarization in the cell as seen by the interacting beam. Possible inhomogeneities of the cell surface and the sample tube, combined with the uncertainty coming from recombination processes, enhance the systematic error of the BRP measurement.

The polarization measurement performed with the PAX detector, however, is sensitive to the *average* total target polarization seen by the beam, including contributions from the residual nuclear polarization of the recombined molecules. Thereby, the PAX detector system, once properly calibrated, offers a way to substantially reduce the systematic errors of the BRP measurement by using it as a relative polarimeter.

Conclusions

A low-energy spin-physics program is pursued at the COSY storage ring of Forschungszentrum Jülich. To support the experimental activity, dedicated tools have been developed in the polarized beam and internal targets sector. Among them, a large acceptance silicon detector suitable for low-energy spin-physics experiments with both beam and/or target polarization has been realized. The detector has been commissioned with an unpolarized proton beam and a polarized deuterium target demonstrating that it can be used for the low-energy spin-physics experimental program at COSY.

Abbreviations

ABS: Atomic Beam Source; ADC: Analog-to-Digital Converter; ANKE: Apparatus for studies of Nucleon and Kaon Ejectiles; BRP: Breit-Rabi Polarimeter; COSY: COoler SYnchrotron; CP: Charge conjugation-Parity; CPLD: Complex Programmable Logic Device; DAQ: Data Acquisition; DC: Direct Current; ECL: Emitter-Coupled Logic; EDM: Electric Dipole Moment; FAIR: Facility for Antiproton and Ion Research; FCT: Fast Current Transformer; FPGA: Field Programmable Gate Array; HV: High Voltage; JULIC: JUelich Light Ion Cyclotron; LIA: Lock-In Amplifier; LV: Low Voltage; LVDS: Low-Voltage Differential Signaling; MSCPV: Milli-Strong CP-Violation; NEG: Non-Evaporable Getter; NIM: Nuclear Instrumentation Module; PAX: Proton-Antiproton eXperiment; PCB: Printed Circuit Board; PDL: Programmable Delay Lines; PPG: Programmable Pulse Generator; QMA: Quadrupole Mass Analyser; RF: Radio-Frequency; SM: Standard Model; RMS: Root Mean Square; SFT: Strong Field Transition; TA: Trigger Amplifier; TGA: Target Gas Analyser; TIVOLI: Time Invariance ViOLating Interactions; UHV: Ultra-High Vacuum; VA: Viking Amplifier; VME: VersaModule Eurocard

Acknowledgements

We express our gratitude to all our colleagues, from various institutions, who have been collaborating for the successful results laid out in this paper.

Authors' contributions

All authors read and approved the final manuscript.

Funding

This work was supported by the ERC Advanced Grant POLPBAR (Grant Agreement 246980), the EU grants of the Projects I3HP2 and I3HP3 (Grant Agreements 227431 and 283286), the COSY-FFE program (41853505-FAIR-009), and the Swedish Research Council (Dnos. 624-2009-224 and 624-2010-5135). N.N. Nikolaev wishes to acknowledge the support from the grant 0033-2019-0005 of the Russian Ministry of Sciences.

Availability of data and materials

Not applicable.

Ethics approval and consent to participate

Not applicable.

Consent for publication

Not applicable.

Competing interests
The authors declare that they have no competing interests.

Author details
[1]Universitá di Ferrara and INFN, 44122 Ferrara, Italy. [2]Institut für Kernphysik, Forschungszentrum Jülich, 52425 Jülich, Germany. [3]High Energy Physics Department, St. Petersburg Nuclear Physics Institute, 188350 Gatchina, Russia. [4]Laboratory of Nuclear Problems, Joint Institute for Nuclear Research, 141980 Dubna, Russia. [5]Helmholtz-Institut für Strahlen- und Kernphysik, 53115 Bonn, Germany. [6]Institute for Advanced Simulation, Forschungszentrum Jülich, 52425 Jülich, Germany. [7]Zentralinstitut für Engineering und Technologie (ZEA-1), Forschungszentrum Jülich, 52425 Jülich, Germany. [8]High Energy Physics Institute, Tbilisi State University, 0186 Tbilisi, Georgia USA. [9]UGS Gerlinde Schulteis and Partner GbR, 08428 Langenbernsdorf, Germany. [10]Landau Institute for Theoretical Physics, 119334 Moscow, Russia. [11]Phys. Institut der Universität Erlangen Nürberg, 91058 Erlangen, Germany. [12]INFN, Sezione di Bari, 70126 Bari, Italy. [13]Department of Physics, Royal Institute of Technology, SE-10691, Stockholm, Sweden. [14]Skobeltsyn Institute of Nuclear Physics, Lomonosov Moscow State University, 119991 Moscow, Russia. [15]Dubna State University, 141980 Dubna, Russia. [16]Department of Physics, Moscow State University, 119991 Moscow, Russia. [17]Zentralinstitut für Systeme der Elektronik (ZEA-2), Forschungszentrum Jülich, 52425 Jülich, Germany. [18]National Centre for Nuclear Research, 00681 Warsaw, Poland.

Received: 24 April 2019 Accepted: 9 July 2019
Published online: 16 August 2019

References

1. Wilkin C (2017) The legacy of the experimental hadron physics programme at COSY. Eur Phys J A 53(6):114. https://doi.org/10.1140/epja/i2017-12295-4
2. Ströher H (2015) Search for electric dipole moments using storage rings (srEDM). Advanced grant of the European Research Council, Proposal number: 694340. available from http://www.sredm-ercgrant.de/sredm/EN/Home/home_node.html
3. Barone V, et al (2005) Antiproton-proton scattering experiments with polarization. https://arxiv.org/abs/hep-ex/0505054
4. Augustyniak W, et al (2012) Polarization of a stored beam by spin-filtering. Phys Lett B 718(1):64–69. https://doi.org/10.1016/j.physletb.2012.10.030
5. Valdau Y, Aksentyev A, Eversheim D, Lorentz B (2016) The physics program of PAX at COSY. J Phys Conf Ser 678(1):012,027. https://doi.org/10.1088/1742-6596/678/1/012027
6. Lenisa P, Rathmann F (2013) Perspectives for polarized antiprotons. Nucl Phys News 23(1):27–30. https://doi.org/10.1080/10619127.2013.767698
7. Krisch AD, Lin AMT, Chamberlain O (1986) Polarized beams at SSC. Proceedings, Workshop, Ann Arbor, USA, June 10-15, 1985 Polarized antiprotons. In: Proceedings, Workshop on polarized antiproton sources, Bodega Bay, USA, April 18-21, 1985. AIP Conf Proc Vol. 145. pp 1–251
8. Chattopadhyay S, Barber DP, Buttimore N, Court G, Steffens E (2008) Polarized antiproton beams - how?. In: Proceedings, International Workshop, Daresbury, UK, August 29-31, 2007. AIP Conf Proc 1008
9. Grosnick DP, et al (1990) The Design and Performance of the Fnal High-energy Polarized Beam Facility. Nucl Instrum Meth:A290:269. https://doi.org/10.1016/0168-9002(90)90541-D
10. Oellers D, Barion L, Barsov S, Bechstedt U, Benati P, Bertelli S, Chiladze D, Ciullo G, Contalbrigo M, Dalpiaz P, Dietrich J, Dolfus N, Dymov S, Engels R, Erven W, Garishvili A, Gebel R, Goslawski P, Grigoryev K, Hadamek H, Kacharava A, Khoukaz A, Kulikov A, Langenberg G, Lehrach A, Lenisa P, Lomidze N, Lorentz B, Macharashvili G, Maier R, Martin S, Merzliakov S, Meshkov I, Meyer H, Mielke M, Mikirtychiants M, Mikirtychiants S, Nass A, Nekipelov M, Nikolaev N, Nioradze M, d'Orsaneo G, Papenbrock M, Prasuhn D, Rathmann F, Sarkadi J, Schleichert R, Smirnov A, Seyfarth H, Sowinski J, Spoelgen D, Stancari G, Stancari M, Statera M, Steffens E, Stein H, Stockhorst H, Straatmann H, Ströher H, Tabidze M, Tagliente G, Engblom PT, Trusov S, Vasilyev A, Weidemann C, Welsch D, Wieder P, Wüstner P, Zupranski P (2009) Polarizing a stored proton beam by spin flip?. Physics Letters B 674(4):269–275. https://doi.org/10.1016/j.physletb.2009.03.037
11. Bystricky J, Lehar F, Winternitz P (1978) Formalism of Nucleon-Nucleon Elastic Scattering Experiments. J Phys France:39:1. https://doi.org/10.1051/jphys:019780039010100
12. Weidemann C, Rathmann F, Stein HJ, Lorentz B, Bagdasarian Z, Barion L, Barsov S, Bechstedt U, Bertelli S, Chiladze D, Ciullo G, Contalbrigo M, Dymov S, Engels R, Gaisser M, Gebel R, Goslawski P, Grigoriev K, Guidoboni G, Kacharava A, Kamerdzhiev V, Khoukaz A, Kulikov A, Lehrach A, Lenisa P, Lomidze N, Macharashvili G, Maier R Martin, Mchedlishvili D Meyer, Merzliakov S, Mielke M, Mikirtychiants M, Mikirtychiants S, Nass A, Nikolaev NN, Oellers D, Papenbrock M, Pesce A, Prasuhn D, Retzlaff M, Schleichert R, Schröer D, Seyfarth H, Soltner H, Statera M, Steffens E, Stockhorst H, Ströher H, Tabidze M, Tagliente G, Engblom PT, Trusov S, Valdau Y, Vasiliev A, Wüstner P (2015) Toward polarized antiprotons: Machine development for spin-filtering experiments. Phys Rev ST Accel Beams 18:020,101. https://doi.org/10.1103/PhysRevSTAB.18.020101. http://link.aps.org/doi/10.1103/PhysRevSTAB.18.020101
13. Eversheim D, Valdau Yu, Lorentz B (2013) Test of time-reversal invariance at COSY (TRIC). Hyperfine Interact 214(1-3):127–132. https://doi.org/10.1007/s10751-013-0778-9
14. Okun LB (1965) Note concerning CP parity. Yad Fiz 1:938–939
15. Prentki J, Veltman MJG (1965) Possibility of CP violation in semistrong interactions. Phys Lett 15:88–90. https://doi.org/10.1016/0031-9163(65)91141-8
16. Lee TD, Wolfenstein L (1965) Analysis of CP Noninvariant Interactions and the K0(1), K0(2) System. Phys Rev 138:B1490–B1496. https://doi.org/10.1103/PhysRev.138.B1490 , [,373(1965)]
17. Okun LB (1967) The Violation of CP Invariance. Sov Phys Usp 9:574–601. https://doi.org/10.1070/PU1967v009n04ABEH003013
18. Bernreuther W (2002) CP violation and baryogenesis. Lect Notes Phys 591:237–293. https://doi.org/10.1007/3-540-47895-7_7

19. Conzett HE (1993) Null tests of time reversal invariance. Phys Rev C48:423–428. https://doi.org/10.1103/PhysRevC.48.423
20. Temerbayev AA, Uzikov YuN (2015) Spin observables in proton-deuteron scattering and T-invariance test. Phys Atom Nucl 78(1):35–42. https://doi.org/10.1134/S1063778815010184, [Yad. Fiz.78,no.1-2,38(2015)]
21. Uzikov YuN Temerbayev (2015) Null-test signal for T-invariance violation in pd scattering. Phys Rev C92(1):014,002. https://doi.org/10.1103/PhysRevC.92.014002,1506.08303
22. Uzikov YuN, Haidenbauer J (2016) Polarized proton-deuteron scattering as a test of time-reversal invariance. Phys Rev C94(3):035,501. https://doi.org/10.1103/PhysRevC.94.035501,1607.04409
23. Beyer M (1989) Time Reversal Invariance in Multipole Mixing Ratios. Nucl Phys A 493:335–349. https://doi.org/10.1016/0375-9474(89)90401-6
24. v Przewoski B, et al (2006) Analyzing powers and spin correlation coefficients for $p + d$ elastic scattering at 135 and 200 MeV. Phys Rev C 74:064,003. https://doi.org/10.1103/PhysRevC.74.064003. http://link.aps.org/doi/10.1103/PhysRevC.74.064003
25. Aksentyev A, Eversheim D, Lorentz B, Valdau Y (2017) The Test of Time Reversal Invariance at Cosy (TRIC). Acta Phys Polon B48:1925. https://doi.org/10.5506/APhysPolB.48.1925
26. Airapetian A, et al (2013) The HERMES Recoil Detector. JINST 8:P05,012. https://doi.org/10.1088/1748-0221/8/05/P05012, 1302.6092
27. Ciullo G, Barion L, Barschel C, Grigoriev K, Lenisa P, Nass A, Sarkadi J, Statera M, Steffens E, Tagliente G (2011) The polarised internal target for the PAX experiment. J Phys Conf Ser 295:012,150. https://doi.org/10.1088/1742-6596/295/1/012150
28. Capiluppi M, Carassiti V, Ciullo G, Lenisa P, Nass A, Steffens E (2014) Dual H and D cavity for the PAX target polarimeter. Phys Part Nucl 45:283–284. https://doi.org/10.1134/S1063779614010171
29. Covo MK (2014) Nondestructive synchronous beam current monitor. Review of Scientific Instruments 85(12):125,106. https://doi.org/10.1063/1.4902903
30. Courtois C, Jamet C, Le Coz W, Ledu G (2014) Intensity control in experimental rooms of the GANIL accelerator. Nucl Instrum Meth A768:112–119. https://doi.org/10.1016/j.nima.2014.09.044
31. Valdau Y, Eltcov L, Mikirtytchiants S, Trusov S, Wuestner P (2017) Development of High Resolution Beam Current Measurement System for COSY-Julich. In: Proceedings, 5th International Beam Instrumentation Conference (IBIC 2016) Barcelona, Spain, September 11-15, 2016, p TUPG41. https://doi.org/10.18429/JACoW-IBIC2016-TUPG41
32. Derbenev YaS, Kondratenko AM, Serednyakov SI, Skrinsky AN, Tumaikin GM, Shatunov YuM (1978) Radiative polarization: Obtaining, control, using. Part Accel 8:115–126
33. Lehrach A, Maier R (2001) Siberian Snake for the Cooler Synchrotron COSY. Conf Proc C0106181:2566–2568. [,2566(2001)]
34. Grigoryev K, et al (2009) Machine studies for the development of storage cells at the ANKE facility of COSY. Nucl Instrum Meth A599:130–139. https://doi.org/10.1016/j.nima.2008.11.006, 0805.2008
35. Baumgarten C, et al (2002) An atomic beam polarimeter to measure the nuclear polarization in the HERMES gaseous polarized hydrogen and deuterium target. Nucl Instrum Meth A482:606–618. https://doi.org/10.1016/S0168-9002(01)01738-7
36. Baumgarten C, et al (2003) A gas analyzer for the internal polarized target of the HERMES experiment. Nucl Instrum Meth A508:268–275. https://doi.org/10.1016/S0168-9002(03)01702-9
37. Schleichert R, Krings T, Mussgiller A, Protic D, Merzlyakov S (2003) A self-triggering silicon-tracking telescope for spectator proton detection. IEEE Trans Nucl Sci 50:301–306. https://doi.org/10.1109/TNS.2003.812431
38. Agostinelli S, et al (2003) GEANT4: A Simulation toolkit. Nucl Instrum Meth A506:250–303. https://doi.org/10.1016/S0168-9002(03)01368-8
39. Ohlsen GG, Keaton PW (1973) Techniques for measurement of spin-1/2 and spin-1 polarization analyzing tensors. Nucl Instrum Meth 109:41–59. https://doi.org/10.1016/0029-554X(73)90450-3

Publisher's Note